Self-Oscillating Wireless Battery Charging Systems With Locking Equilibrium Points

Jiayu Zhou, Jiayang Wu, *Member, IEEE*, Yuzhi Yang, Siew Chong Tan, *Fellow, IEEE*, and Shu-Yuen Ron Hui, *Fellow, IEEE*

***Abstract*—This article presents a self-oscillating control method with locking equilibrium points for series-series compensated wireless power transfer (WPT) systems designed for battery charging. Previous studies indicate that frequency bifurcation in the WPT system reveals three zero-phase angle (ZPA) frequency points, which act as equilibrium points in self-oscillating systems. This phenomenon can cause the system to switch between different ZPA points, potentially leading to fluctuations in output power, current oscillation, or instability. The analysis in this article focuses on the frequency characteristics of the WPT system under battery/voltage loads, highlighting significant differences compared to systems with resistance loads. Notably, multiple equilibrium points exist only within a narrow range of input impedance angles. A self-oscillating control strategy is proposed to lock the WPT system at a specified equilibrium point by comparing the designed sending side current to generate pulsewidth modulation signals. The locked equilibrium point is positioned close to the highest ZPA frequency point, ensuring robust misalignment tolerance and near-maximum power output. Moreover, the approach enables zero-voltage switching across the entire operational range. The effectiveness of the proposed method is validated through both simulation and experimental results.**

***Index Terms*—Battery charging, locking equilibrium points, wireless power transfer (WPT), zero-phase angle (ZPA) points.**

I. Introduction

WIRELESS power transfer (WPT) systems leveraging magnetic resonant coupling have emerged as a promising technology for battery charging. By eliminating the need for physical connections, this technology enhances operational flexibility and safety, making it particularly attractive for sectors such as consumer electronics [1], medical devices [2], and electric public transportation systems [3], [4], [5]. Among the different configurations, the series-series (SS) compensation topology, often implemented with a diode rectifier/synchronous rectifier on the receiving end, stands out due to its balance of efficiency, simplicity, and cost-effectiveness [6]. As the demand for efficient and reliable charging solutions continues to grow, it becomes imperative to explore innovative strategies to optimize SS-compensated WPT systems, particularly in the context of battery charging applications.

To minimize reactive power and reduce the volt-ampere rating of components, WPT systems are typically operated at zero-phase-angle (ZPA) frequencies. A detailed analysis of ZPA points in WPT systems was first conducted in 2004 [7], identifying the conditions for frequency bifurcation, which indicates the existence of three distinct ZPA points. The approximate maximum power output capabilities of the system under bifurcation conditions were also discussed. Subsequently, numerous studies have been conducted to explore the complexities of bifurcation, such as its effects on control strategies [8], methods for its avoidance [9], and critical conditions for wireless battery charging systems [10]. Based on the analysis of systems exhibiting bifurcation, it was further demonstrated in [11] that symmetric WPT systems exhibit remarkable misalignment tolerance at the lowest or highest ZPA frequencies, as established through electric circuit theory. This conclusion has been further supported by findings from coupled mode theory [12]. Recently, a thorough evaluation of the accuracy and limitations of these two models was performed from a ZPA perspective in [13], concluding that electric circuit theory remains the more accurate analytical tool for studying near-field WPT systems. Therefore, in this article, we will utilize electric circuit modeling to further analyze WPT systems exhibiting bifurcation, to ensure a high level of precision in the findings.

The finding that WPT systems with frequency bifurcation exhibit remarkable misalignment tolerance at the lowest or highest ZPA frequencies has generated increased interest in their applications under variable coupling coefficient conditions [11], [12]. Rapid and stable locking onto the ZPA point is essential for WPT systems that experience real-time coupling coefficient alterations. Drawing from earlier techniques used in resonant converters [14], self-oscillating methods have been employed to automatically lock the ZPA point in WPT systems. In such systems, voltage and current remain in phase during each switching cycle, inherently aligning the system's equilibrium point with the ZPA point. This automatic tracking approach provides numerous benefits, including simplicity, low cost, and swift response.

Received 25 February 2025; revised 11 May 2025 and 7 July 2025; accepted 7 August 2025. Date of publication 18 August 2025; date of current version 22 October 2025. This work was supported in part by the Hong Kong RGC General Research Fund 172120025 and in part by the Hong Kong RGC Theme-based Research Project under Grant T23-708/24-N. Recommended for publication by Associate Editor O. Lucia. *(Corresponding author: Jiayang Wu.)*

Jiayu Zhou, Jiayang Wu, Yuzhi Yang, and Siew Chong Tan are with the Department of Electrical Engineering, City University of Hong Kong, Hong Kong (e-mail: jiayzhou@cityu.edu.hk; jiayang.wu@cityu.edu.hk; yuzhiyang4-c@my.cityu.edu.hk; siewctan@cityu.edu.hk).

Shu-Yuen Ron Hui is with the Department of Electrical Engineering, City University of Hong Kong, Hong Kong, and also with the Department of Electrical and Electronics Engineering, Imperial College London, SW7 2BX London, U.K. (e-mail: eeronhui@cityu.edu.hk).

Color versions of one or more figures in this article are available at https://doi.org/10.1109/TPEL.2025.3599675.

Digital Object Identifier 10.1109/TPEL.2025.3599675

Self-oscillating control does not require information from the other side of the WPT, but the need for communication depends on system requirements and coordinated control strategies.

Recently, many studies have delved into self-oscillating WPT systems, investigating various compensation structures such as series-series [15], parallel-parallel [16] topologies, and other compensation configurations [17], [18]. Moreover, self-oscillating control strategies have been combined with modulation methods, such as phase-shift modulation [19], [20] and pulse-density modulation [21], to further regulate the system's output. Self-oscillating techniques have also been applied to WPT systems featuring switch-controlled capacitors [22] or variable inductance [23]. However, current research primarily concentrates on the application of self-oscillating methods in different WPT configurations and the evaluation of their misalignment tolerance capabilities. A significant gap in the literature exists regarding the frequency characteristics and design considerations of self-oscillating WPT systems. When the system exhibits bifurcation, it indicates the presence of three equilibrium points, two of which possess asymptotic stability characteristics [19]. Self-oscillating WPT systems generally lack additional constraints, allowing the final operating point to be located at either of the two stable equilibrium points, and are influenced by the initial conditions, load changes, and disturbances [20], [24]. The potential for switching between different equilibrium points can result in power fluctuations and even system oscillations, which also significantly broaden the operational frequency range. In some instances, the system may even demonstrate the coexistence of both split frequencies [25], [26]. To achieve stability, a method for locking equilibrium points has been applied to amplifier-type oscillators [26], but it is not suitable for switching-mode inverters operating at medium to high power levels. Additionally, existing discussions on self-oscillating methods have been primarily centered around resistance loads, overlooking the increasing application of battery charging in WPT systems.

Given the complexities introduced by frequency bifurcation in WPT systems, particularly in terms of stability and dynamic performance at multiple ZPA points, this article aims to establish a robust self-oscillating control strategy that maintains the system at a targeted equilibrium point. The frequency characteristics of WPT systems with voltage loads are thoroughly examined, indicating that the operational range of bifurcation phenomena is relatively limited. The proposed strategy effectively locks the equilibrium point near the highest ZPA frequency while successfully avoiding the bifurcation region. This significantly enhances the system's robustness and enables the inverter to operate at zero-voltage switching (ZVS) throughout the entire operational range. In doing so, self-oscillating WPT systems are prevented from switching between different equilibrium points, and their operational frequency range is substantially reduced. Moreover, the proposed system also retains the desirable characteristics of the ZPA points, such as near-maximum power output and excellent misalignment tolerance. The proposed control strategy and method of analysis are validated through comprehensive simulation and experimental results.

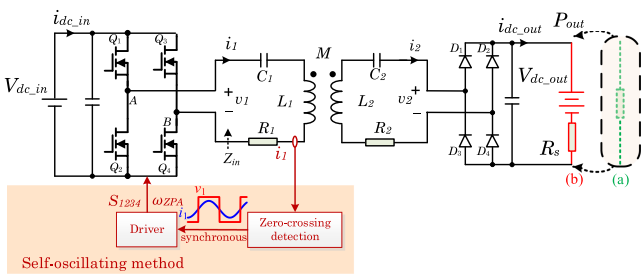

Fig. 1. SS-compensated WPT system with (a) resistance load or (b) voltage load.

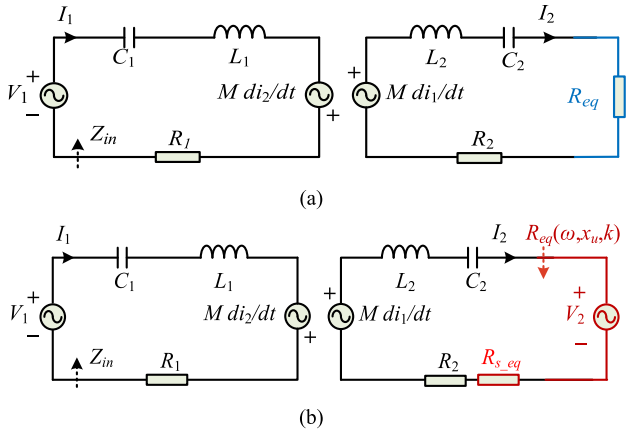

Fig. 2. Equivalent circuit of the SS-compensation WPT system using FHA. (a) Resistance load. (b) Voltage load.

II. Basics for Self-Oscillating WPT Systems With Resistance Loads or Voltage Loads

Fig. 1 shows a typical configuration of an SS-compensated WPT system using the self-oscillating method. The variables of the system are defined as such: v_1 and v_2 represent the sending and pickup voltages, respectively, i_1 and i_2 denote the currents flowing through the sending and pickup coils, R_1 and R_2 indicate the equivalent parasitic resistances of the sending and pickup sides, R_s indicate the battery's internal resistance, M signifies the mutual inductance, and Z_{in} is the input impedance of the system. Moreover, L_1 and L_2 represent the inductances, whereas C_1 and C_2 denote the capacitances on the sending and pickup sides, satisfying the relationship $\omega_p = \frac{1}{\sqrt{L_1 C_1}}; \omega_s = \frac{1}{\sqrt{L_2 C_2}}$.

Two common load types in WPT systems are shown in Fig. 1, where the dashed line represents a resistance load, and the solid line represents a voltage load. Based on the fundamental harmonic approximation (FHA), their equivalent circuits are shown in Fig. 2. For the system incorporating a diode rectifier with a resistance load, the equivalent output load (R_{eq}) can be calculated as follows:

$$R_{\text{eq}} = \frac{8}{\pi^2} R_L \tag{1}$$

where R_L is the output load value of the system. Therefore, the output load of the equivalent circuit can be considered constant, irrespective of the system's frequency characteristics. In contrast, the equivalent circuit for a WPT system with a

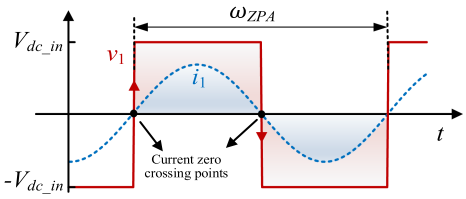

Fig. 3. Synchronization of sending voltage and current in WPT systems with the self-oscillation method.

voltage load is shown in Fig. 2(b) [27]. Due to the characteristics of the diode rectifier, the output of this equivalent circuit exhibits the following features:

$$\begin{cases} |V_2| = \frac{4}{\pi} V_{\text{dc\_out}} \\ \angle V_2 = \angle I_2 \end{cases} \tag{2}$$

where $V_{\text{dc·out}}$ represents the output dc voltage. It is important to note that a battery load is a classic voltage load, where the voltage is primarily influenced by the battery's state of charge. The battery's internal resistance can be represented on the ac side as an equivalent small resistor $R_{s\cdot\text{eq}}$, which has minimal impact on the system. Therefore, the load in Fig. 2(b) can be effectively approximated as a voltage load, and its fluctuation range aligns with the battery voltage fluctuation range. The subsequent discussions in this article will be based on the battery load. For the steady-state analysis of the operating point under consideration, the battery load can be represented by a fixed equivalent resistance R_{eq}, simplifying the analysis without loss of generality. However, in self-oscillating WPT systems, the operating frequency varies during dynamic response. Therefore, the equivalent output load should be regarded as a frequency-dependent equivalent load $R_{\text{eq}}(\omega)$, where the condition specified in (2) must be consistently satisfied.

The self-oscillating control method is increasingly utilized in WPT systems with varying coupling coefficients due to its excellent misalignment tolerance. The typical configuration of such a system is shown in Fig. 1. The sending side current i_1 is sampled, and the zero-crossing points of the current are measured. When the sending current crosses from negative to positive, the output voltage of the inverter rises from $-V_{\text{in}}$ to V_{in}, as shown in Fig. 3. Conversely, when the sending current crosses from positive to negative, the inverter's output voltage transitions from V_{in} to $-V_{\text{in}}$. In this configuration, the system's sending voltage and current remain in phase, minimizing reactive power flow and ensuring a high efficiency. Therefore, the equilibrium points of the self-oscillating system should satisfy the condition that the input impedance angle (θ_{input}) is 0, where

$$\theta_{\text{input}} = \arctan \frac{\text{Im}(Z_{\text{in}})}{\text{Re}(Z_{\text{in}})}. \tag{3}$$

In the WPT system with a resistance load, as shown in Fig. 2(a), the ZPA frequency points have been extensively studied [7]. When the system satisfies the condition specified in the following equation, it exhibits a bifurcation phenomenon that

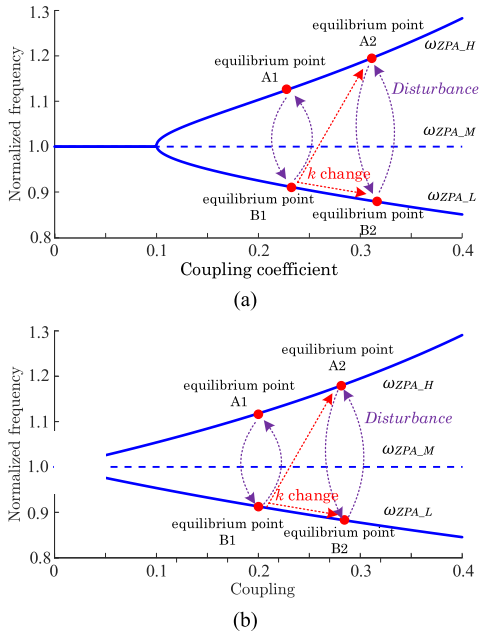

Fig. 4. Relationship between ZPA frequencies and coupling coefficient. (a) Resistance load with $Q_s = 10$. (b) Battery load with $x_u = 0.9$.

results in the emergence of three distinct ZPA points:

$$k > \frac{1}{Q_S}\sqrt{1 - \frac{1}{4Q_S^2}} \tag{4}$$

where k is the coupling coefficient and Q_s represents the quality factor of the pickup side and can be expressed as $Q_S = \frac{\omega_0 L_2}{R_2 + R_{\text{eq}}}$.

Conversely, when condition (4) is not met, only a single ZPA point is observed at the resonant frequency. For the WPT system with a battery load, the conditions necessary for the system to exhibit three ZPA points are as follows [10]:

$$x_u < 1 \tag{5}$$

where x_u is the unbalanced factor, defined as $x_u = \sqrt{\frac{L_1}{L_2}}\frac{V_2}{V_1}$. It is evident that, unlike WPT systems with resistance loads, the conditions for the existence of bifurcation phenomena in systems with battery loads are primarily influenced by x_u and are largely independent of k. It should be noted that the effect of parasitic resistance is disregarded in the derivation of (5), necessitating a typical design margin of about 1% –3% in typical system design. Based on the analysis of the ZPA frequencies [7], [10], the equilibrium points of the self-oscillating WPT system with either a resistance load or a battery load under self-oscillating control are shown in Fig. 4. When the system with a resistance load satisfies the conditions of (4), or when the system with a battery load meets the conditions of (5), the system undergoes frequency bifurcation, resulting in three ZPA points ($\omega_{\text{ZPA}\cdot H}$, $\omega_{\text{ZPA}\cdot M}$, $\omega_{\text{ZPA}\cdot L}$), with $\omega_{\text{ZPA}\cdot M}$ corresponding to the resonant frequency point [10].

Self-oscillating WPT systems are typically designed to operate within a bifurcation region to achieve excellent misalignment tolerance [11]. In this scenario, the system has three equilibrium points, with stability occurring only at both $\omega_{\text{ZPA}\cdot H}$ and

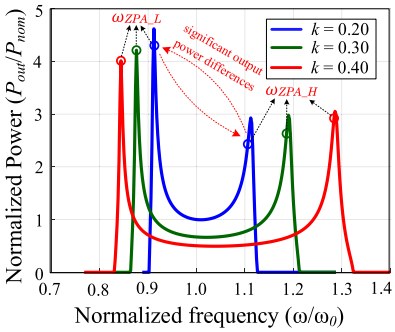

Fig. 5. Frequency characteristics of the asymmetric IPT system with battery load for $x_u = 0.95$ and $\omega_s = 1.005\omega_p$.

$\omega_{\mathrm{ZPA}\cdot L}$ [19]. Thus, the self-oscillating system can operate at either of these two equilibrium points. Depending on initial conditions, load variations, or disturbances, the system may switch between different equilibrium points [26]. This can lead to frequent oscillations and shifts in operating points, significantly expanding the operating frequency range, as shown in Fig. 4. Furthermore, previous studies have demonstrated that the exceptional misalignment tolerance capability of self-oscillating WPT systems frequently hinges on the premise of parity symmetry, enabling the system's output power to remain remarkably consistent across all of the $\omega_{\mathrm{ZPA}\cdot L}$ and $\omega_{\mathrm{ZPA}\cdot H}$ points. However, achieving this consistency in mass production environments poses a significant challenge. Notably, even a minor deviation of just 0.5% in the resonant frequency between the sending and pickup sides can result in a substantial difference in the system's output power at $\omega_{\mathrm{ZPA}\cdot L}$ and $\omega_{\mathrm{ZPA}\cdot H}$, as shown in Fig. 5. It is crucial to acknowledge that this observation excludes the influence of voltage drop and parasitic parameters of the diode within the receiving-side rectifier, which typically exert minimal influence in high-voltage systems. Therefore, stabilizing the equilibrium point of the self-oscillating system at either $\omega_{\mathrm{ZPA}\cdot L}$ or $\omega_{\mathrm{ZPA}\cdot H}$ enhances robustness and stability while reducing the operational frequency range. Although existing methods for fixing the equilibrium point are applicable to amplifier-type oscillators [26], they are unsuitable for switching-mode inverters operating at medium to high power levels. This article analyzes the frequency characteristics of WPT systems with battery loads, highlighting differences from those with resistance loads. Based on the unique frequency characteristics of the WPT system with battery loads, a method for stabilizing the system's equilibrium point in self-oscillating WPT systems is proposed.

III. Frequency Characteristics of WPT Systems With Self-Oscillating Methods

In WPT systems with self-oscillating control, analyzing the system's equilibrium point and corresponding frequency characteristics is essential. By applying Kirchhoff's voltage law on the equivalent circuit shown in Fig. 2, the following relationships can be derived:

$$\begin{cases} \mathbf{V}_1 = R_1\mathbf{I}_1 + j\omega L_1\mathbf{I}_1 - j\omega M\mathbf{I}_2 + \frac{\mathbf{I}_1}{j\omega C_1} \\ \mathbf{V}_2 = R_{\mathrm{eq}}(\omega)\mathbf{I}_2 = -R_2\mathbf{I}_2 - j\omega L_2\mathbf{I}_2 + j\omega M\mathbf{I}_1 - \frac{\mathbf{I}_2}{j\omega C_2}. \end{cases} \tag{6}$$

TABLE I
Simulation and Experimental Parameters of the WPT System

Parameter	Symbol	Value
Input voltage	V_{in}	10 V
Battery voltage	$V_{\mathrm{dc\_out}}$	7–9 V
Resonant frequency	f_p	85 kHz
Coupling coefficient	k	0.1–0.3
Self-inductance of the primary-side coil	L_1	46 μH
Self-inductance of the secondary-side coil	L_2	46 μH
AC resistance of the primary side	R_1	0.09 Ω
AC resistance of the secondary side	R_2	0.09 Ω
MOSFETs	---	EPC 2071

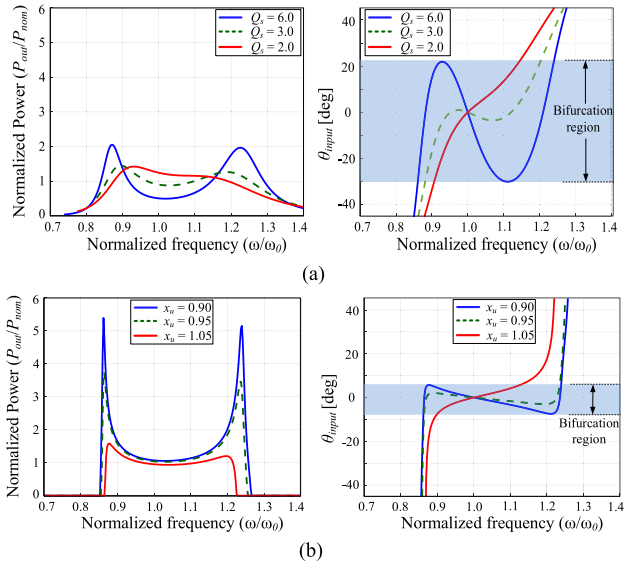

Fig. 6. Frequency characteristic of WPT systems with $k = 0.35$ for (a) resistance loads and (b) battery loads.

For WPT systems with resistance loads, R_{eq} is unaffected by the operating frequency and is solely determined by (1). In contrast, for systems with battery loads, $R_{\mathrm{eq}}(\omega)$ is significantly affected by the operating frequency, necessitating a careful design of its application in self-oscillating WPT systems. By solving (1)–(3) and (6) and utilizing the parameters provided in Table I, the frequency characteristics of the WPT system with both resistance and battery loads can be analyzed, with the results shwn in Fig. 6. In the WPT system with a resistance load and $k = 0.35$, a bifurcation phenomenon occurs when Q_s exceeds 2.8, meeting the condition stated in (4). Similarly, in the WPT system with a battery load, bifurcation arises upon satisfying the condition in (5). It is crucial to note that the presence of three equilibrium points does not solely occur when the input impedance angle is zero; rather, it spans over a specific range of input impedance angles. This aspect has often been overlooked in previous studies, particularly in the context of self-oscillating WPT systems.

To maintain a high system's efficiency and mitigate excessive voltage across the resonant capacitor, the maximum power range discussed in this article is set at three times the power of the system when it is operating at the resonant frequency. The system with a resistance load exhibits bifurcation across a broader range

of input impedance angles, as shown in Fig. 6(a). In contrast, the system with a battery load experiences bifurcation within a much narrower range, as indicated by the results in Fig. 6(b). This suggests that in most wireless battery charging applications, it is feasible to design the system at a specified operating point outside the bifurcation region shown in Fig. 6(b). In such cases, the operating point can be positioned close to the highest ZPA frequency point. Therefore, the designed self-oscillating system avoids multiple equilibrium points that could lead to switching between different operating points, while still achieving good misalignment tolerance, high efficiency, and near-maximum power output.

IV. Designed Self-Oscillating WPT Systems With Locking Equilibrium Points

A. Implementation of the Presented Method

To achieve good misalignment tolerance characteristics and maximum power output, self-oscillating WPT systems are often unknowingly mis-designed to operate within the bifurcation region predetermined by (4) or (5) [11], [12]. As explained, multiple equilibrium points exist in this situation, which lead to potentially random and nonstatic switching of the equilibrium points in dynamical operating conditions or under disturbances. Therefore, the locking of the system's equilibrium point during the process of the WPT is crucial, as it enhances robustness and narrows the operating frequency range.

Based on the frequency characteristics analysis of the system with battery loads, bifurcation occurs when the condition in (5) is met. Notably, the phenomenon of multiple equilibrium points exists only within a narrow range of input impedance angles, as shown in Fig. 6(b). This observation underscores the feasibility and convenience of redesigning the system's equilibrium point for self-oscillating WPT systems, as it is not always necessary for the system to operate precisely at the frequently analyzed ZPA point. To avoid the bifurcation region and concurrently achieve ZVS across the entire operating range, the equilibrium point can be positioned slightly above $\omega_{\mathrm{ZPA}\cdot H}$, as shown in Fig. 7(a). In this scenario, the system's equilibrium point remains locked near the highest ZPA frequency, as shown in Fig. 7(b), even when k varies in real-time or experiences disturbances. Operating at this designed equilibrium point allows the system to evade the bifurcation region while maintaining the characteristics similar to those of a ZPA point, such as having good misalignment tolerance and operating at near-maximum power output. Another advantage is that the input impedance angle at the newly designed equilibrium point can remain low while achieving ZVS, minimizing reactive power flow, and ensuring a high efficiency.

To ensure that the self-oscillating WPT system operates at the designed equilibrium point, a self-oscillating control method that achieves equilibrium point locking is proposed in this article. The implementation block diagram of this control method is shown in Fig. 8. The control involves a current sensor for sensing i_1, two comparators, two signal-and-hold operators, and a pulsewidth modulation (PWM) generator to output the driving signals S_{1234}. The controller can be easily realized in analog or

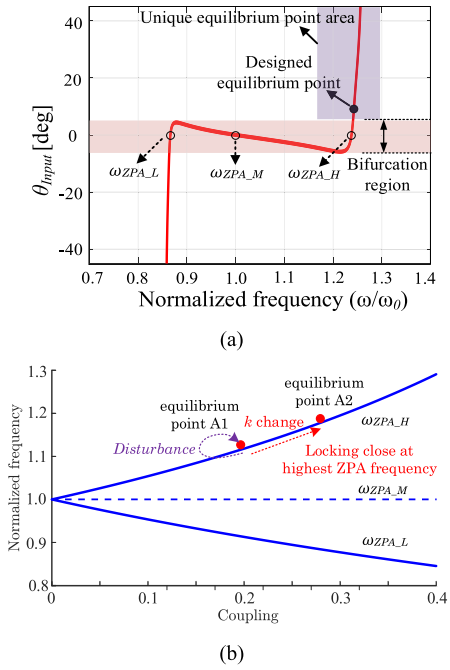

Fig. 7. Designed equilibrium points for self-oscillating WPT systems with battery loads. (a) Designed scheme. (b) Trajectory of the equilibrium points under coupling changes or other perturbations.

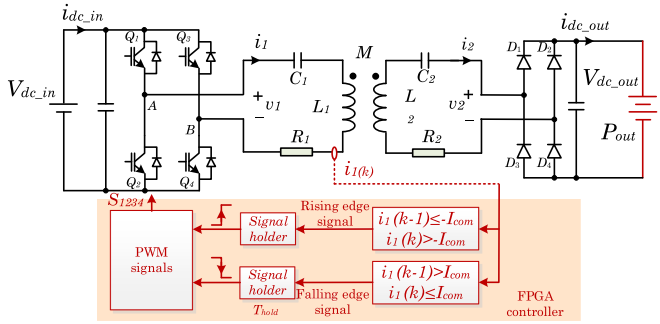

Fig. 8. Implementation of the proposed self-oscillating method for locking the equilibrium point.

digital form, and the operating process is as follows. The system continuously samples the sending current i_1 and compares it with a reference current value (I_{com}) to generate the PWM signals to drive the power inverter. When the previously sampled current $i_1(k\text{-}1)$ is below $-I_{\mathrm{com}}$ and the sampled current $i_1(k)$ is above $-I_{\mathrm{com}}$, the inverter's output switches from $-V_{\mathrm{in}}$ to V_{in}. Conversely, when $i_1(k\text{-}1)$ is above I_{com} and $i_1(k)$ is below I_{com}, the inverter output changes from V_{in} to $-V_{\mathrm{in}}$. With this control, the system's input impedance is adjusted to be slightly inductive, thereby positioning the equilibrium point frequency to be slightly above $\omega_{\mathrm{ZPA}\cdot H}$. The specific value of I_{com} is meticulously designed to achieve ZVS while avoiding the bifurcation region of the input impedance angle θ_{input}. Fig. 9(a) shows the waveforms of the sending voltage and sending current of the WPT system with the implemented self-oscillating control method. The sending current exhibits a slight phase lag relative to the sending voltage, which is aligned with the input impedance angle designed to avoid the bifurcation region. However, high-frequency current

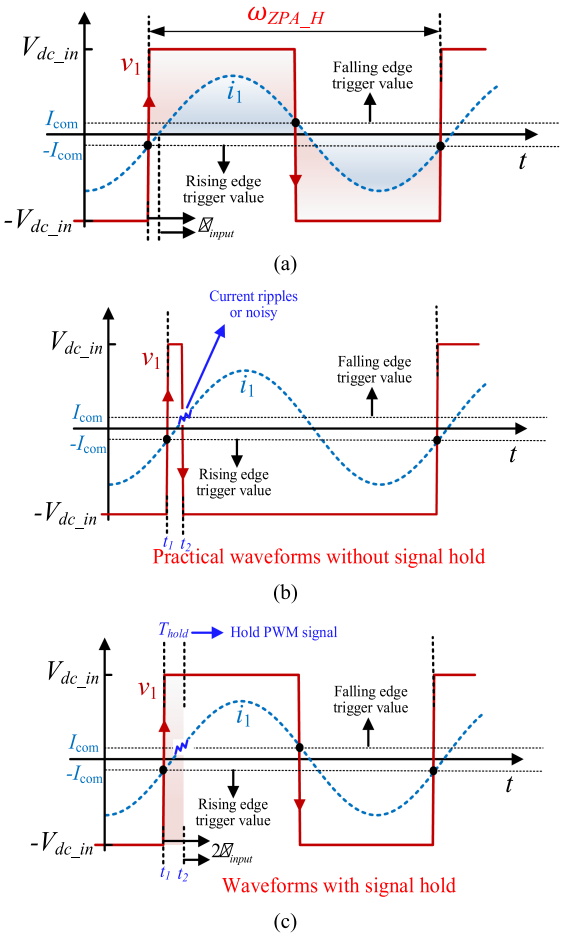

Fig. 9. Sending voltage and current of the system with the implemented self-oscillating method. (a) Ideal waveforms. (b) Possible waveforms resulting from current ripples and sampling noise. (c) Waveform analysis following a brief hold PWM signal of Fig. 8.

ripple or sampling noise may interfere with the implementation of self-oscillating control. At time t_1, the instantaneous value of the ac current reaches -$I_{\rm com}$ and begins to increase, triggering the rising edge. The current then continues to rise to $I_{\rm com}$ at time t_2. Ideally, the current is increasing, and the falling edge should not be triggered according to the rule shown in Fig. 8. However, due to potential ripples and sampling noise, the instantaneous current may momentarily decrease at $I_{\rm com}$, triggering the falling edge, as shown in Fig. 9(b).

Thus, a hold design is essential to mitigate the effects of current ripples and noise. The hold time encompasses the duration required for the instantaneous ac current to transition from -$I_{\rm com}$ to $I_{\rm com}$, as shown in Fig. 9(c). In this manuscript, this hold time should be designed as

$$T_{\rm hold} > t_2 - t_1 = \frac{2\cdot\theta_{\rm input}}{360}\cdot\frac{1}{f_s} = \frac{\theta_{\rm input}}{180}\cdot\frac{1}{f_s}. \tag{7}$$

The designed $\theta_{\rm input}$ in this manuscript is 8°. Additionally, the switching frequency f_s of the proposed method exceeds the resonant frequency. Thus, $T_{\rm hold}$ should be greater than approximately 523 ns based on (7). Additionally, considering the operating frequency range of the system, which spans from

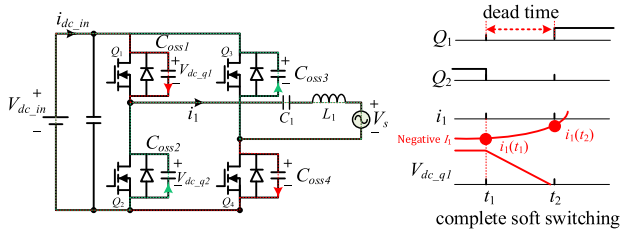

Fig. 10. Complete ZVS process of MOSFETs.

85 to 150 kHz, it is essential that the $T_{\rm hold}$ time remains less than half of the system's maximum frequency as follows:

$$T_{\rm hold} < \frac{T_{\rm min}}{2} = \frac{1}{2f_{s\_\max}}. \tag{8}$$

This criterion ensures that the $T_{\rm hold}$ duration does not adversely affect the normal operation of the system, as it is grounded in frequencies that are above the typical operational range. Based on the parameters designed in this study, $T_{\rm hold}$ should be between 500 and 3333 ns, as derived from (7) and (8). To enhance the robustness of the system without compromising its normal operating range, $T_{\rm hold}$ can be designed to be approximately 2000 ns, which represents the midpoint between 500 and 3333 ns. This adjustment provides a sufficient margin for the parameters defined in (7) and (8). This technique eliminates potential erroneous PWM signals that may arise from multiple current zero crossings due to ripples or noise. Therefore, the designed self-oscillating WPT system circumvents the complexities associated with multiple equilibrium points ($\omega_{\rm ZPA\cdot H}$, $\omega_{\rm ZPA\cdot M}$, $\omega_{\rm ZPA\cdot L}$), while preserving the advantages of the self-oscillating system at the $\omega_{\rm ZPA\cdot H}$ point.

B. Design of Control Parameter

Based on Fig. 7, the objective is to design a new equilibrium point that allows the system to achieve ZVS while avoiding the bifurcation region. Therefore, a detailed discussion on the conditions for achieving this newly conceived equilibrium point, considering these dual objectives, is essential.

To achieve ZVS operation across the full working range, the voltage across the MOSFETs must approach zero before their turn-ON. This condition can be met by ensuring that a negative sending current value I_1 is present to discharge the parasitic equivalent output capacitance ($C_{\rm oss}$) of the MOSFET before turn-ON. For the sake of simplicity in analyzing ZVS, it is commonly assumed that the inverter attains ZVS when the inverter's sending current slightly lags its sending voltage. However, this assumption can sometimes lead to incomplete ZVS [28]. In practical scenarios, to guarantee that V_{ds-q2} descends to zero completely when Q_2 is switched ON, as shown in Fig. 10, the freewheeling interval with the inductor current during dead time must fulfill specific conditions [29] given as:

$$\frac{1}{2}L_e[i_1^2(t_1) - i_1^2(t_2)] \geq 2Q_{\rm oss}(V_{\rm dc\_in})V_s \tag{9}$$

where $Q_{\rm oss}$ is the stored charge of the parasitic output capacitances of the MOSFET during its turn-OFF. $i_1(t_1)$ and $i_1(t_2)$ are the values of the primary-side current i_1 at the beginning and end

of the dead zone, respectively. V_s is the equivalent primary load voltage, which can be estimated from Fig. 2 and (6). L_e is the energy-equivalent inductance, which can be expressed as [29]

$$L_e = L_1 - \frac{Q^2_{i_1(Vds)}}{\left(i_1^2(t_1) - i_1^2(t_2)\right) C_1} \tag{10}$$

To address the variability of minimum dead time with changing operating conditions [29], the analysis is simplified by setting the dead time to a larger fixed value (70 ns), ensuring a sufficient margin. Moreover, careful consideration must be given to designing I_{com} to avoid the bifurcation region under standard operating conditions. It is worth noting that the system power at the ZPA frequency is close to the maximum power level transmissible with the system, with the difference influenced by the coupling coefficient and system parameters. In the design process, consider that the output power of the self-oscillating WPT system is limited to three times the output power of the system when operating at the resonant frequency. By solving (2) and (6), $R_{\text{eq}}(\omega)$ can be calculated for the system with battery loads. Assuming the resonant frequency on both sides of the system is equal to ω_0 and by omitting negligible components of R_1 and R_2, $R_{\text{eq}}(\omega)$ can be derived as given in (11), shown at the bottom of this page.

Moreover, the input impedance angle θ_{input} of the system can be determined by solving (3), (6), and (11). For conciseness, we can adopt an accurate but simpler form of the equation by neglecting the parasitic resistances R_1 and R_2, which is given as follows (12) shown at the bottom of this page.

It can be observed that the input impedance angle is not solely influenced by L_1, L_2, V_1, and V_2; instead, it is determined by their interrelationship x_u. Therefore, this article primarily addresses the variation of x_u to encompass the entire operating range, including the realization of different output power levels. Finally, (11) and (12) are solved to ascertain the value of the minimum positive input impedance angle, which does not exhibit multiple equilibrium points under various coupling coefficients and output power scenarios. The calculated results are plotted and shown in Fig. 11. P_{res} is the output power value of the system at the resonant frequency when the coupling is at its lowest. This value serves as a benchmark for establishing the output power range. By combining (12) and Fig. 11, it can be calculated that the designed minimum input impedance angle (θ_{design}) is approximately 8°. It is important to emphasize that this value is available across all parameter conditions shown in Fig. 11, as it always surpasses the input impedance angle in the bifurcation area under varying coupling coefficient and output power. In this scenario, I_{com} can be derived as follows:

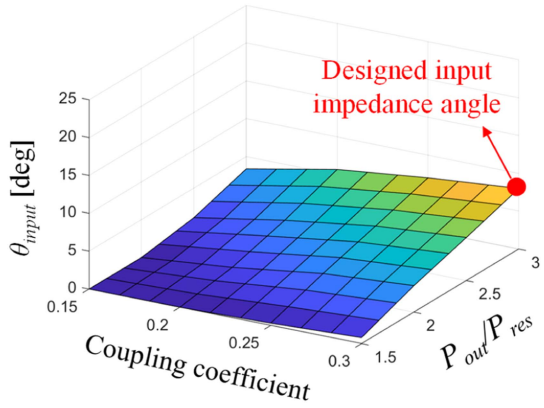

Fig. 11. Maximum input impedance angle values in the bifurcation region under varying coupling coefficient and output power.

$$I_{\text{com}} = \max[I_{1\_\text{zvs}}(t_1), I_{1\_\text{peak}} \cdot \sin(\theta_{\text{design}})] \tag{13}$$

where $I_{\_\text{zvs}}(t_1)$ is the minimum value of $I_1(t_1)$ that satisfies (9) and $I_{1\text{-peak}}$ represents the peak sending current amplitude captured by the system in each switching cycle. Based on the parameters used in this article, the design to avoid bifurcation has encompassed the area necessary for achieving ZVS. Therefore, the subsequent experiments are conducted in accordance with $\theta_{\text{design}} = 8°$. It should be noted that the core component of the sending current is mainly the fundamental component in the coupling coefficient range discussed, as the system operates close to the ZPA point, which is near the maximum power point.

C. Simulation Results

To verify the effectiveness of the proposed method, a simulation model was developed using MATLAB/Simulink. Fig. 12 shows the simulation results of the proposed self-oscillating system. The self-oscillating control is initiated at 3 ms and encounters a significant sampling disturbance at 5 ms. Lasting for 0.03 ms, with an amplitude comparable to the actual current amplitude. During this period, the sampled current can be considered entirely chaotic, with specific results shown in Fig. 12(b). The sampled ripple current becomes excessively large, leading to multiple zero crossings, which results in an increased PWM frequency. Consequently, the system's current amplitude decreases. When the sampling returns to normal, the system stabilizes rapidly within 1 ms. Fig. 12(c) shows the system's input phase angle, which quickly returns to the nonbifurcation area after the disturbance, as the system has only one unique equilibrium point. Thus, the operating frequency of

$$\begin{aligned} R_{\text{eq}}(\omega, x_u, k) &\approx L_2 \cdot \frac{x_u \sqrt{(k^2 - x_u^2)\omega^4 + (2x_u^2 - R_1^2)\omega_0^2\omega^2 - x_u^2\omega_0^4} \cdot ((k^2-1)\omega^4 + (2 + R_2^2)\omega_0^2\omega^2 - \omega_0^4)}{\omega\left[(k^2 - x_u^2)\omega^4 + 2\omega_0^2\omega^2 x_u^2 - x_u^2\omega_0^4\right]} \\ &= L_2 f\left(x_u, k, \omega, R_1, R_2\right). \end{aligned} \tag{11}$$

$$\theta_{\text{input}} \approx \arctan\left(\frac{(\omega_0^2 - \omega^2)\left[(k^2-1)\omega^4 + (2\omega_0^2 - f^2\left(x_u, k, \omega, R_1, R_2\right))\omega^2 - \omega_0^4\right]}{k^2\omega^5 f\left(x_u, k, \omega, R_1, R_2\right)}\right). \tag{12}$$

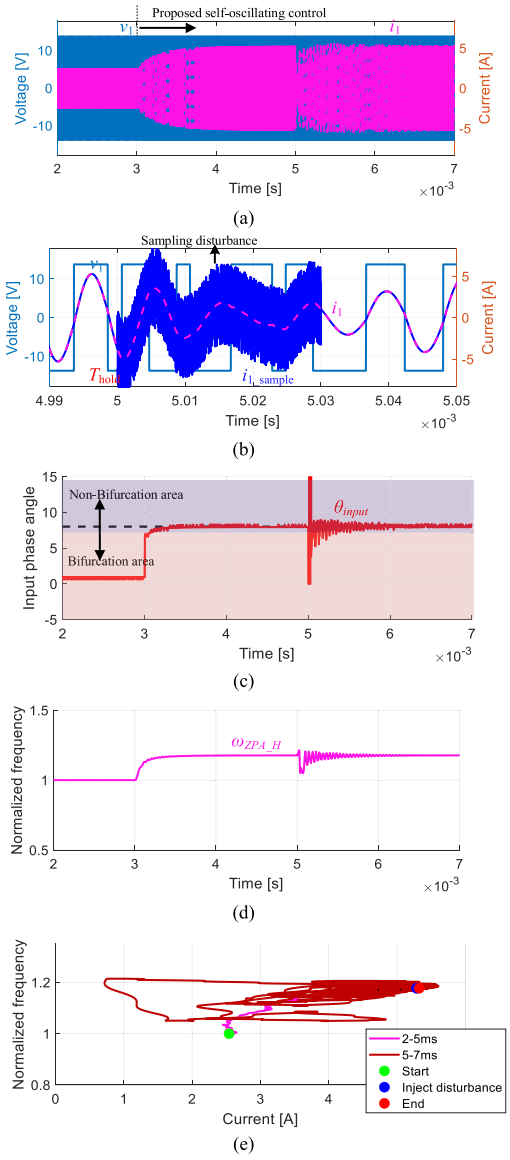

Fig. 12. Simulation results of the proposed self-oscillating system with a sampling disturbance injected at 5 ms. (a) Overall process. (b) Sending-side voltage (v_1), current (i_1), and sample current ($i_{1\text{·sample}}$). (c) Input phase angle. (d) Normalized operation frequency. (e) Operation trajectory.

the system is also rapidly locked at $\omega_{\text{ZPA·}H}$, with no tendency to operate at the subresonant frequency once the disturbance ends, as shown in Fig. 12(d). The trajectory diagram of the system, shown in Fig. 12(e), clearly shows the entire operational process. Notably, the actual current amplitude does not exhibit overshoot, and the frequency consistently remains near $\omega_{\text{ZPA·}H}$, which is above the resonant frequency range.

The proposed system remains consistently locked near $\omega_{\text{ZPA·}H}$, even after experiencing substantial disturbances. This behavior can be attributed to the designed control strategy, which enables the system to avoid the bifurcation area and stabilize at the sole equilibrium point shown in Fig. 7. Moreover, the proposed method possesses strong anti-interference capabilities and robustness due to the presence of T_{hold}.

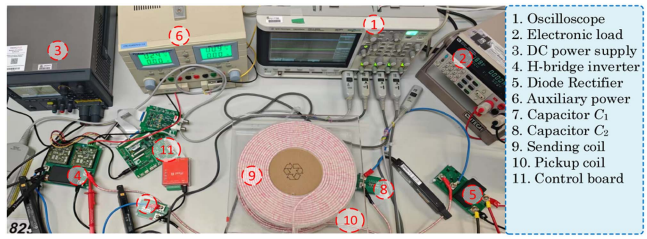

Fig. 13. Prototype of the WPT system for experimental verification.

V. Experimental Results

To validate the aforementioned theoretical analysis, experimental work is conducted using a laboratory prototype designed with parameters specified in Table I (see Fig. 13). The input side of the prototype is connected to a dc voltage source, whereas the output side is linked to an electronic load operating in constant voltage mode to emulate a battery. Typically, a Li-ion battery cell has a voltage range of 3.7–4.35 V [21]. The experiments simulated two Li-ion battery cells connected in series, with an assumed voltage of 7–9.0 V.

The current is collected via a current transformer, and its proportional instantaneous value is obtained through a differential amplifier circuit. This signal is then converted into a digital format using an ADC circuit and subsequently fed into the FPGA. The implementation details within the FPGA are outlined in Figs. 8 and 9. The controller employed in this study is a Cyclone IV EP4CE10 FPGA. Although the controller typically experiences time jitter and PWM timing precision issues, these effects are generally much smaller than 10 ns [30] and can be considered negligible for the system operating around 100 kHz. It is important to acknowledge that high-frequency noise or offsets may be present during the sampling process, leading to fluctuations in the input impedance angle of the system around its designated value. To ensure that the system remains entirely within the nonbifurcation range, it is advisable to maintain a margin for θ_{design} such that the final value is slightly higher than the calculated value shown in Fig. 11. This small adjustment can enhance the robustness of the system while exerting minimal impact on its efficiency and normal operation, given the relatively small magnitude of θ_{design}.

Fig. 14 shows the experimental results of the traditional self-oscillation system. First, the system loses ZVS as the input phase angle is controlled at 0, which also leads to voltage spikes during the turn-ON of the MOSFETs. The system, featuring three equilibrium points, must fulfill the conditions specified in (5). When inductance on both sides is nearly symmetrical and the input voltage exceeds the output voltage, the self-oscillating system exhibits three ZPA points. Therefore, the system exhibits different stable equilibrium points, as shown in Fig. 14(a) and (b). The green line in the figures represents the system's operating frequency, calculated by an FPGA controller that measures the time difference between two rising edges of the PWM signal and is displayed on an oscilloscope via a DAC. The initial frequency refers to the fixed frequency at which the system operates initially before transitioning to self-oscillation control. It can be observed that different initial frequencies may cause

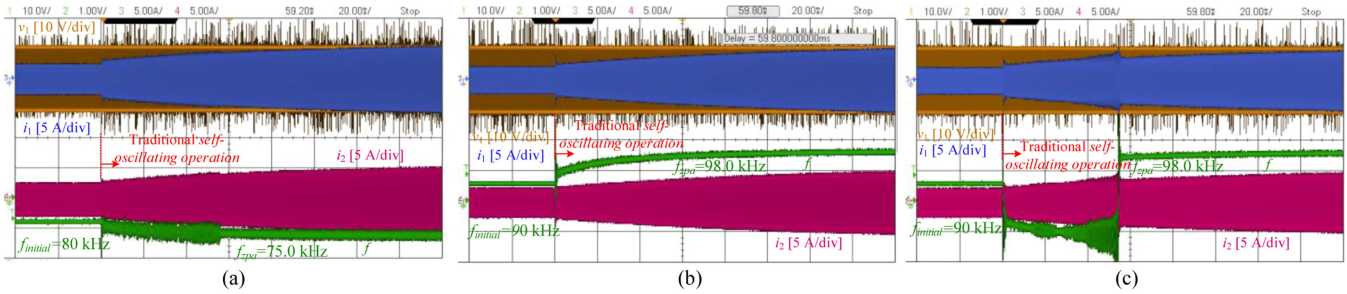

Fig. 14. Dynamic results of the WPT system ($k = 0.27$) with the traditional self-oscillating control under different initial conditions. (a) $f_{\text{initial}} = 80$ kH. (b) $f_{\text{initial}} = 90$ kHz (results 1). (c) $f_{\text{initial}} = 90$ kHz (results 2).

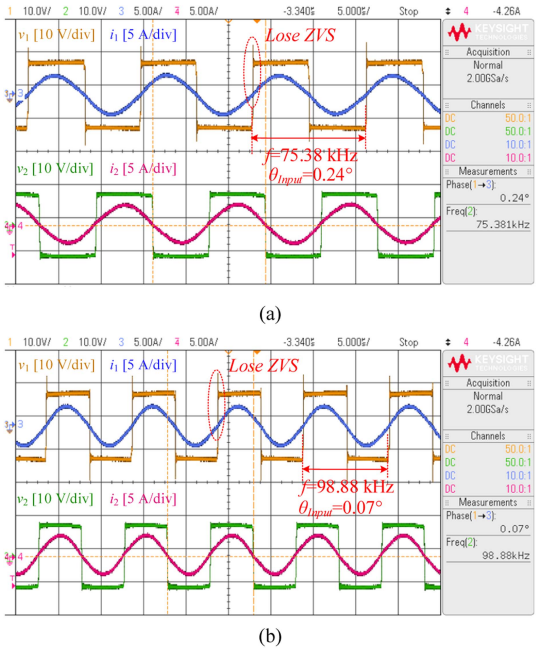

Fig. 15. Self-oscillating WPT system with $k = 0.27$ and $\theta_{\text{design}} = 0°$. (a) $f_{\text{initial}} = 80$ kHz. (b) $f_{\text{initial}} = 90$ kHz.

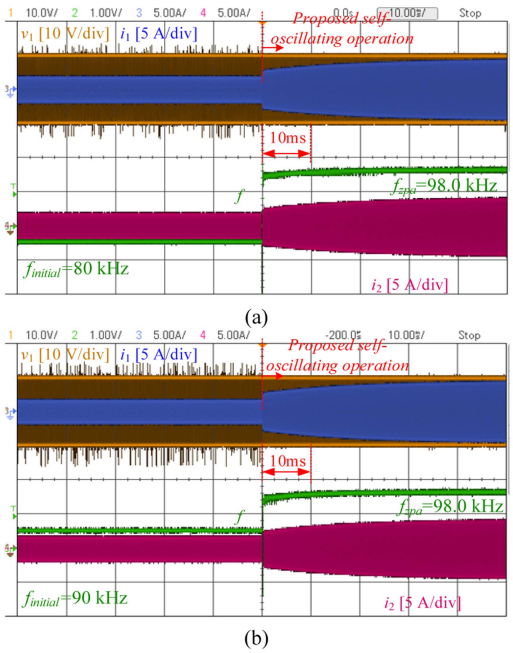

Fig. 16. Dynamic results of the WPT system ($k = 0.27$) with the proposed self-oscillating control under different initial conditions. (a) $\theta_{\text{design}} = 8°$ and $f_{\text{initial}} = 80$ kHz. and (b) $\theta_{\text{design}} = 8°$ and $f_{\text{initial}} = 90$ kHz.

the self-oscillating system to operate at various ZPA frequency points, and after disturbances, it may fluctuate and switch between these points. Although the initial conditions in Fig. 14(b) and (c) are the same, the results from different attempts are not entirely consistent. This variation occurs because the system has two stable equilibrium points, and it can operate at either one, depending on factors such as disturbances or initial conditions. Fig. 15 shows the steady-state results of the WPT system with the traditional self-oscillating control at the lowest and highest ZPA points. It can be observed that the input impedance angles of the system are around 0°, but different equilibrium points exist, as shown in Fig. 15(a) and (5). Moreover, the system cannot achieve ZVS when operating at the ideal ZPA frequency.

Fig. 16 shows the experimental results of the proposed self-oscillating WPT system under various initial conditions. Regardless of whether the initial frequency is in the subresonant or super-resonant frequency region, the system consistently stabilizes rapidly at $\omega_{\text{ZPA}\cdot H}$ within 10 ms after the initiation of self-oscillating control, with no overshoot. This behavior demonstrates the system's remarkable stability and robustness. Unlike the traditional method shown in Fig. 14, which exhibits switching between different equilibrium points, the proposed system has only one equilibrium point. Therefore, initial conditions or disturbances do not affect the system's stability. Additionally, the system achieves ZVS throughout the entire dynamic process, as evidenced by the absence of voltage spikes in the sending voltage waveform.

Fig. 17 shows the steady-state experimental results of the proposed system at various battery voltages. Although the system satisfies the conditions outlined in (5), which indicates three ZPA equilibrium points, the proposed system operates at the designed equilibrium point. It can be observed that the system stabilizes its operating point near $\omega_{\text{ZPA}\cdot H}$, demonstrating robust performance and avoiding $\omega_{\text{ZPA}\cdot L}$. The input impedance angle closely aligns with the designed value ($\theta_{\text{design}} = 8°$) across all input voltage levels. Furthermore, the system reliably achieves ZVS. A zoomed-in waveform of the system during the switching process, highlighting the current and voltage zero-crossing

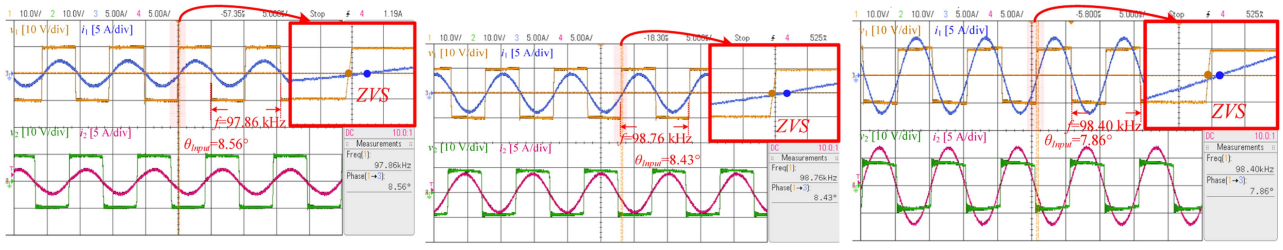

(a) (b) (c)

Fig. 17. Proposed self-oscillating WPT system with $k = 0.27$ and $\theta_{\text{design}} = 8°$. (a) $V_{\text{dc·out}} = 9$ V. (b) $V_{\text{dc·out}} = 8$ V. (c) $V_{\text{dc·out}} = 7$ V.

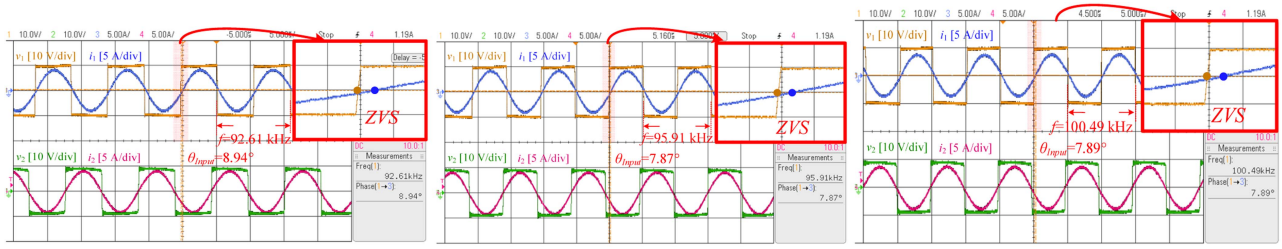

(a) (b) (c)

Fig. 18. Proposed self-oscillating WPT system with $V_{\text{in}} = 10$ V and $\theta_{\text{design}} = 8°$. (a) k= 0.295. (b) $k = 0.221$. (c) $k = 0.15$.

points, is illustrated in the upper right corner of Fig. 17. It is evident that before the turn-ON of the MOSFET, the instantaneous value of i_1 remains consistently negative, indicating that the parasitic equivalent output capacitance of the MOSFET is discharged before turn-ON. Additionally, just before the current crosses zero, the voltage V_{ds} is already at 0, confirming the successful realization of complete ZVS.

Fig. 18 shows the experimental results of the proposed system under different coupling coefficient conditions. As expected, the system stabilizes near $\omega_{\text{ZPA·}H}$ and achieves ZVS for the different conditions. Notably, Fig. 18 also shows the system's excellent misalignment tolerance. Despite a significant change in coupling coefficient, the input and output currents remain almost constant, with only the operating frequency shifting.

Fig. 19 compares the performance of the traditional system and the proposed system during changes in the coupling coefficient. Fig. 19(a) shows the dynamic behavior of the traditional system. As the coupling coefficient varies from 0.29 to nearly around 0.15 and returns to 0.29, the system's operating frequency transitions from the super-resonant to the sub-resonant frequency region. This indicates that conventional systems may operate at either of these two ZPA points, influenced by external disturbances. Fig. 19(b) shows the dynamic process of the proposed system as the coupling coefficient changes from 0.29 to around 0.15 and returns to 0.29. Notably, the system remains consistently locked near $\omega_{\text{ZPA·}H}$, demonstrating remarkable robustness. Additionally, the system maintains ZVS throughout this dynamic process.

Fig. 20 shows the experimental results of both the conventional and proposed self-oscillating WPT systems under parameter deviations ($\omega_s \approx 1.015\omega_p$). The coupling coefficient changes

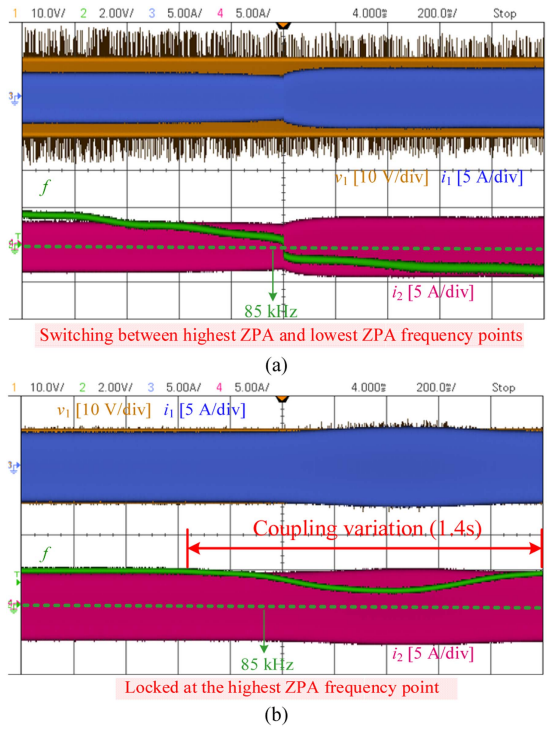

(a)

(b)

Fig. 19. Dynamic results of the WPT system ($\omega_s \approx 1.0\omega_p$) under real-time variation of coupling (changes from 0.29 to 0.15 and returns to 0.29). (a) Results using the traditional self-oscillating control. (b) Results using the proposed self-oscillating control method with $\theta_{\text{design}} = 8°$.

from 0.29 to approximately 0.15 and then returns to 0.29, with the entire process lasting about 600 ms. The traditional approach may switch from the highest ZPA frequency point to the lowest due to coupling disturbances, resulting in substantial output

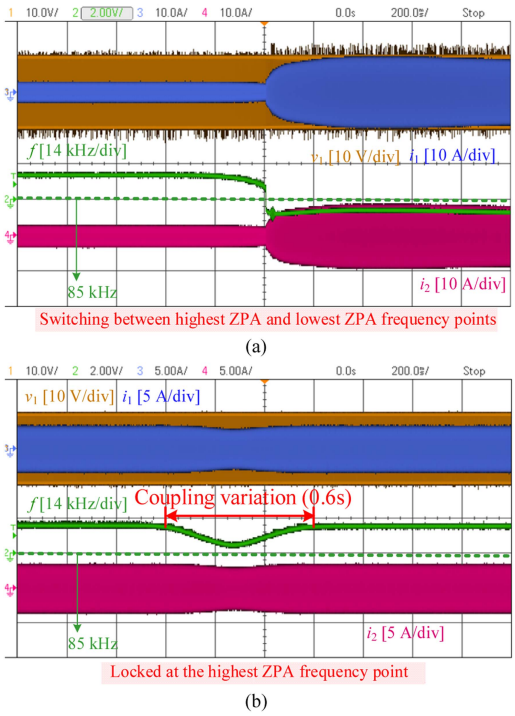

Fig. 20. Dynamic results of the WPT system ($\omega_s \approx 1.015\omega_p$) under real-time variation of coupling (changes from 0.29 to 0.15 and returns to 0.29). (a) Results using the traditional self-oscillating control. (b) Results using the proposed self-oscillating control method with $\theta_{\text{design}} = 8°$.

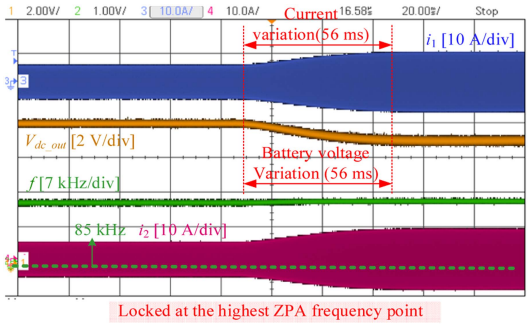

Fig. 21. Proposed self-oscillating WPT system with $\theta_{\text{design}} = 8°$ responds to real-time variations in battery voltage.

power fluctuations, as shown in Fig. 20(a). The slight asymmetry between the two sides results in substantial differences in their output power, aligning with the conclusions drawn from Fig. 5. In contrast, our proposed method successfully locks the system to the highest ZPA frequency point, leading to smaller output power fluctuations and demonstrating enhanced robustness and stability, as shown in Fig. 20(b).

To further show the anti-interference capability and robustness of the proposed method, Fig. 21 shows experimental data illustrating real-time changes in battery voltage. Although the output voltage of the electronic load is set to step from 8 to 7 V, this process lasts approximately 56 ms due to the inherent limitations of the electronic load's response speed. Upon stabilization of the output voltage, the self-oscillating control system also stabilizes, showing no overshoot in current and consistently locking near $\omega_{\text{ZPA}\cdot H}$. The static and dynamic experimental results presented validate the effectiveness of the proposed method. The proposed approach locks the equilibrium point, significantly enhancing the system's robustness while considerably reducing the operating frequency range. Notably, the newly designed equilibrium point is located near the original ZPA points, thus retaining the characteristics of near-maximum power output and excellent misalignment tolerance.

VI. Conclusion

This article presents a self-oscillating method for locking equilibrium points in SS-compensated WPT systems specifically designed for battery charging. By analyzing the frequency characteristics of the WPT system under battery loads, a region of multiple equilibrium points for the input impedance angles has been identified, confined to a narrow range. A new equilibrium point is designed to avoid the bifurcation region of the input impedance angle, positioned slightly above the highest ZPA frequency point. This approach effectively prevents the self-oscillating system from switching between different ZPA points while ensuring robust misalignment tolerance and near-maximum power output. Moreover, the proposed system enables ZVS with minimal turn-OFF current across the entire operational range. Experimental results demonstrate that the system's operating point remains locked to the designed equilibrium points, showcasing its robustness under dynamic coupling coefficient conditions, varying initial conditions, and perturbations.

References

[1] S. Y. Hui, "Planar wireless charging technology for portable electronic products and Qi," *Proc. IEEE*, vol. 101, no. 6, pp. 1290–1301, Jun. 2013.
[2] D. Ahn and S. Hong, "Wireless power transmission with self-regulated output voltage for biomedical implant," *IEEE Trans. Ind. Electron.*, vol. 61, no. 5, pp. 2225–2235, May 2014.
[3] G. A. Covic and J. T. Boys, "Modern trends in inductive power transfer for transportation applications," *IEEE J. Emerg. Sel. Topics Power Electron.*, vol. 1, no. 1, pp. 28–41, Mar. 2013.
[4] S. Li and C. C. Mi, "Wireless power transfer for electric vehicle applications," *IEEE J. Emerg. Sel. Topics Power Electron.*, vol. 3, no. 1, pp. 4–17, Mar. 2015.
[5] G. Guidi, J. A. Suul, F. Jenset, and I. Sorfonn, "Wireless charging for ships: High-power inductive charging for battery electric and plug-in hybrid vessels," *IEEE Electrific. Mag.*, vol. 5, no. 3, pp. 22–32, Sep. 2017.
[6] Y. Zhang, S. Chen, X. Li, and Y. Tang, "Design of high-power static wireless power transfer via magnetic induction: An overview," *CPSS Trans. Power Electron. Appl.*, vol. 6, no. 4, pp. 281–297, Dec. 2021.
[7] C. S. Wang, G. A. Covic, and O. H. Stielau, "Power transfer capability and bifurcation phenomena of loosely coupled inductive power transfer systems," *IEEE Trans. Ind. Electron.*, vol. 51, no. 1, pp. 148–157, Feb. 2004.
[8] U. Iruretagoyena, A. Garcia-Bediaga, L. Mir, H. Camblong, and I. Villar, "Bifurcation limits and non-idealities effects in a three-phase dynamic IPT system," *IEEE Trans. Power Electron.*, vol. 35, no. 1, pp. 208–219, Jan. 2020.
[9] K. Aditya and S. S. Williamson, "Design guidelines to avoid bifurcation in a series–series compensated inductive power transfer system," *IEEE Trans. Ind. Electron.*, vol. 66, no. 5, pp. 3973–3982, May 2019.
[10] J. Zhou, C. Q. Jiang, T. Ma, G. Guidi, X. Zhang, and J. A. Suul, "Comprehensive analysis of bifurcation and frequency splitting phenomena in inductive battery charging systems," *IEEE Trans. Power Electron.*, vol. 39, no. 11, pp. 15329–15341, Nov. 2024.
[11] F. Mastri, A. Costanzo, and M. Mongiardo, "Coupling-independent wireless power transfer," *IEEE Microw. Wireless Compon. Lett.*, vol. 26, no. 3, pp. 222–224, Mar. 2016.
[12] S. Assawaworrarit, X. Yu, and S. Fan, "Robust wireless power transfer using a nonlinear parity–time-symmetric circuit," *Nature*, vol. 546, no. 7658, pp. 387–390, Jun. 2017.

[13] J. Wu, K. Li, J. Zeng, and S.-Y. R. Hui, "On the limitations of the coupled mode theory and parity-time symmetry for near-field wireless power transfer research," *IEEE Trans. Power Electron.*, vol. 39, no. 5, pp. 6433–6441, May 2024.
[14] H. Pinheiro, P. K. Jain, and G. Joos, "Self-sustained oscillating resonant converters operating above the resonant frequency," *IEEE Trans. Power Electron.*, vol. 14, no. 5, pp. 803–815, Sep. 1999.
[15] J. Zhou, B. Zhang, W. Xiao, D. Qiu, and Y. Chen, "Nonlinear parity-time-symmetric model for constant efficiency wireless power transfer: Application to a drone-in-flight wireless charging platform," *IEEE Trans. Ind. Electron.*, vol. 66, no. 5, pp. 4097–4107, May 2019.
[16] J. Liu, X. Qu, Y. Li, and C. Ma, "Investigation of PT-symmetric frequency and compensation for IPT coupling-independent CC/CV and efficiency in wide load range," *IEEE Trans. Power Electron.*, vol. 38, no. 11, pp. 13353–13362, Nov. 2023.
[17] Z.-J. Liao, Q.-W. Zhu, Y. Yu, C.-Y. Xia, and C.-C. Rong, "Analysis and design of self-oscillating magnetic coupling wireless power transfer systems," *IEEE J. Emerg. Sel. Topics Power Electron.*, vol. 12, no. 1, pp. 1140–1149, Feb. 2024.
[18] Z. Wei, B. Zhang, S. Lin, and C. Wang, "A self-oscillation WPT system with high misalignment tolerance," *IEEE Trans. Power Electron.*, vol. 39, no. 1, pp. 1870–1887, Jan. 2024.
[19] A. Namadmalan, "Self-oscillating pulsewidth modulation for inductive power transfer systems," *IEEE J. Emerg. Sel. Topics Power Electron.*, vol. 8, no. 2, pp. 1813–1820, Jun. 2020.
[20] Y. Gu, J. Wang, Z. Liang, and Z. Zhang, "Communication-free power control algorithm for drone wireless in-flight charging under dual-disturbance of mutual inductance and load," *IEEE Trans. Ind. Inform.*, vol. 20, no. 3, pp. 3703–3714, Mar. 2024.
[21] D. Wu, R. Mai, S. Zhao, Z. He, and F. Peng, "A self-oscillating controller based on pulse density modulator in wireless power transfer," in *Proc. IEEE Energy Convers. Congr. Expo.*, 2019, pp. 2125–2128.
[22] L. Wu, B. Zhang, and Y. Jiang, "A misalignment-tolerant autonomous wireless power transfer system for battery charging based on detuning control," *IEEE Trans. Power Electron.*, vol. 39, no. 3, pp. 3851–3863, Mar. 2024.
[23] B. Cheng, L. He, and H. Liu, "Constant output wireless power transfer system via variable inductance and synchronous control under high misalignment," *IEEE J. Emerg. Sel. Topics Power Electron.*, vol. 12, no. 3, pp. 3226–3235, Jun. 2024.
[24] Z. Hua, K. T. Chau, W. Liu, and X. Tian, "Pulse frequency modulation for parity-time-symmetric wireless power transfer system," *IEEE Trans. Magn.*, vol. 58, no. 8, Aug. 2022, Art. no. 8002005.
[25] H. J. Reich, J. G. Skalnik, and J. D. Crane, "Simultaneous oscillation at two or more frequencies," *Proc. IEEE*, vol. 51, no. 7, pp. 1051–1052, Jul. 1963.
[26] G. Feng and J.-J. Sit, "An injection-locked wireless power transfer transmitter with automatic maximum efficiency tracking," *IEEE Trans. Ind. Electron.*, vol. 68, no. 7, pp. 5733–5743, Jul. 2021.
[27] G. Guidi and J. A. Suul, "Minimizing converter requirements of inductive power transfer systems with constant voltage load and variable coupling conditions," *IEEE Trans. Ind. Electron.*, vol. 63, no. 11, pp. 6835–6844, Nov. 2016.
[28] M. Kasper, R. M. Burkart, G. Deboy, and J. W. Kolar, "ZVS of power MOSFETs revisited," *IEEE Trans. Power Electron.*, vol. 31, no. 12, pp. 8063–8067, Dec. 2016.
[29] C.-T. Truong and S.-J. Choi, "Improved ZVS criterion for series resonant converters," *IEEE Access*, vol. 12, pp. 5333–5344, 2024.
[30] Intel Corporation, "Cyclone IV EP4CE10 FPGA," 2010. [Online]. Available: https://www.intel.com/content/www/us/en/products/sku/210464/cyclone-iv-ep4ce10-fpga/specifications.html

Jiayu Zhou received the B.Eng. and M.S. degrees in electrical engineering from Beijing Jiaotong University, Beijing, China, in 2016 and 2019, respectively, and the Ph.D. degree in engineering cybernetics from the Norwegian University of Science and Technology, Trondheim, Norway, in 2023.

He is currently a Postdoctoral Research Fellow with City University of Hong Kong, Hong Kong. His research interests include wireless power transfer and power converters for renewable energy systems.

Jiayang Wu (Member, IEEE) received the B.Eng. degree in electrical information engineering from Zhejiang University, Hangzhou, China, in 2017, and the Ph.D. degree in electrical and electronic engineering from The University of Hong Kong, Hong Kong, in 2022.

She was a Research Fellow with the School of Electrical and Electronic Engineering, Nanyang Technological University, Singapore, in 2023. Since 2024, she has been a Research Assistant Professor with the Department of Electrical and Electronic Engineering, The University of Hong Kong.

Prof. Wu was a recipient of She was a recipient of the Best Paper Award (Second Place) of the IEEE TRANSACTIONS ON POWER ELECTRONICS in 2019 and 2023, the Best Presentation Award at the IEEE Applied Power Electronics Conference and Exposition (APEC) in 2024, and the Best Paper Awards at the IEEE Conference on Industrial Electronics & Applications (ICIEA) and International Zhejiang Power Electronics Conference (ZPEC) in 2025. She also holds two Chinese patents and one U.S. patent. Her research interests include wireless power transfer, electric vehicle charging, resonant converters, and renewable energy.

Yuzhi Yang received the B.Eng. degree from Harbin Institute of Technology, Harbin, China, in 2019, and the M.Eng. degree from Shanghai Jiao Tong University, Shanghai, China, in 2022, both in electrical engineering. He is currently working toward the Ph.D. degree in electrical engineering with City University of Hong Kong, Hong Kong.

His research interests include wireless power transfer and dc–dc converters.

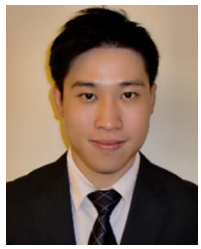

Siew Chong Tan (Fellow, IEEE) received the B.Eng. (Hons.) and M.Eng. degrees in electrical and computer engineering from the National University of Singapore, Singapore, in 2000 and 2002, respectively, and the Ph.D. degree in electronic and information engineering from the Hong Kong Polytechnic University, Hong Kong, in 2005.

From September to October 2009, he was a visiting scholar with the Grainger Center for Electric Machinery and Electromechanics, University of Illinois at Urbana-Champaign and an Invited Academic Visitor of Huazhong University of Science and Technology, Wuhan, China, in 2011. He is currently a Chair Professor with the Department of Electrical Engineering, City University of Hong Kong, Hong Kong. His research interests include the areas of power electronics and control, LED lighting, smart grids, and clean energy technologies.

Shu-Yuen Ron Hui (Fellow, IEEE) received the B.Sc. (Eng.) Hons. degree in electrical and electronic engineering from the University of Birmingham, Birmingham, U.K., in 1984, and the D.I.C. and Ph.D. degrees in electrical engineering from Imperial College London, London, U.K., in 1987.

He held academic positions with the University of Nottingham and the University of Sydney, and an endowed professorship with the University of Hong Kong. He is currently a Chair Professor of Power Electronics with the City University of Hong Kong, Hong Kong, and Imperial College London. He has authored or coauthored more than 500 research papers, including 330 refereed journal publications. According to IEEE Xplore, his patent citations exceed 1260. More than 125 of his patents have been adopted by industry worldwide. His inventions on wireless charging platform technology underpin key dimensions of Qi, the world's first wireless power standard, with freedom of positioning and localized charging features for wireless charging of consumer electronics. He also developed the Photo-Electro-Thermal Theory for LED Systems and Electric Spring technology for smart grid. His research interests include power electronics, wireless power, sustainable lighting, and smart grid.

Prof. Hui is a Fellow of the Australian Academy of Technology & Engineering, the US National Academy of Inventors, and the Royal Academy of Engineering, U.K. He was the recipient of the IEEE Rudolf Chope R&D Award and the IET Achievement Medal (The Crompton Medal) in 2010, the IEEE William E. Newell Power Electronics Award in 2015, and the IET JJ Thomson Medal in 2024.